In situ compression study of taper-free metallic glass nanopillars

Kuzmin, O. V.; Pei, Y. T.; de Hosson, J. T. M.

Published in:
Applied Physics Letters

DOI:
10.1063/1.3598400

In situ compression study of taper-free metallic glass nanopillars

O. V. Kuzmin, Y. T. Pei, and J. T. M. De Hosson[a)]
Department of Applied Physics, Zernike Institute for Advanced Materials and Materials Innovation Institute M2i, University of Groningen, Nijenborgh 4, 9747 AG Groningen, The Netherlands

(Received 20 February 2011; accepted 17 May 2011; published online 7 June 2011)

Because tapering leads to inevitable artifacts in the analyses of compression experiments on micrometer sized pillars, in this study taper-free nanosized pillars of Zr-based metallic glass of $Zr_{61.8}Cu_{18}Ni_{10.2}Al_{10}$ composition with diameter ranging from 600 to 90 nm were fabricated. These pillars were compressed *in situ* in a transmission electron microscope as a function of pillar diameter. Under compression each pillar of large diameter exhibits predominant inhomogeneous and intermittent plastic flow characterized by shear banding (SB) events. However, pillars around 150 nm in diameter and below show homogeneous deformation during compression without SB. © *2011 American Institute of Physics*. [doi:10.1063/1.3598400]

Metallic glass (MG) belongs to a technologically interesting class of materials that was intensively investigated during the last couple of decades.[1] Due to the absence of microstructural features like grain-boundaries or heterophase boundaries that are typical for crystalline materials, MGs exhibit excellent properties, such as high yield strength, advantageous soft and hard magnetic properties, high corrosion resistance and biocompatibility.[2] However, at room temperature MGs are not ductile and tend to fail in a brittle fashion when loaded either in compression or tension,[3] which limits their applicability.

In bulk MGs plastic deformation is concentrated in extremely thin, sheetlike volumes known as shear bands (SBs) and a relevant question is whether and how nucleation and propagation of these SBs are affected by the external size of the system. Do we face extrinsic or intrinsic size effects and would it be possible to suppress brittleness and enhance ductility just by changing the size of the samples?[4] Size effect—or the lack thereof—during deformation of nanosized MG objects has recently drawn great attention. It is not only of fundamental interests when scrutinizing shear localization processes in MGs, but also of practical significance for the incorporation of small sized MG components in micro-/nanoelectromechanical systems.[5] Despite the number of recent publications dealing with compression of focused ion beam (FIB) fabricated micropillars, consensus does not seem to exist on size effects in either strength or modes of deformation of MGs. These controversies are largely related to the *ex situ* tests methods when deformation events cannot be correlated with the particular individual SBs.[6]

Another issue of concerns is that tapering is inevitable for FIB-milled MG pillars with diameters down to submicrometer scale, as highly localized SBs may preferentially nucleate at the corner of sample-plunger contact during compression.[7–15] In literature tapering angles range between 2°–3.5° and 7°–15° and may cause that the deformation always starts at the top leading to the so-called mushrooming effect. Our previous study has shown that tapering has a large influence on the deformation behavior making stress analysis rather difficult.[16,17] These effects become more serious in smaller pillars.

Besides size effects addition of alloying elements that lower the ratio between shear modulus (μ) and bulk modulus (B) may help in alleviating brittleness. MGs with $\mu/B > 0.41-0.43$ (or, equivalently, with Poisson's ratio $\nu < 0.31-0.32$) are more brittle.[18] This correlation applies equally for as-cast MGs of different compositions. In this letter, Al addition was chosen to improve the ductility of MG in bulk state instead of Ti addition in previously investigated $Zr_{50}Ti_{16.5}Cu_{15}Ni_{18.5}$. *In situ* transmission electron microscope (TEM) compression observations of taper-free micro-/nanopillars of Zr-based MG of $Zr_{61.8}Cu_{18}Ni_{10.2}Al_{10}$ composition and diameters ranging from 600 to 90 nm are presented. It is revealed that the deformation is defect-nucleation-controlled in larger pillars but becomes propagation-controlled in smaller pillars.

Nontapered nanopillars were fabricated by FIB in a FIB/SEM microscope (Lyra, Tescan, CZ) from Zr-based MG ribbons of $Zr_{61.8}Cu_{18}Ni_{10.2}Al_{10}$ composition prepared by melt spinning. Micro-wedges out of these ribbons with length about 100 μm and thickness 2–5 μm were prepared by mechanical polishing. A set of taper-free nanopillars with diameters ranging from 600 to 90 nm was fabricated by using a combination of top and side FIB milling. First a series of rectangular microsized beams were milled on the microwedge. Then out of these beams, nanopillars [Fig. 1(a)]

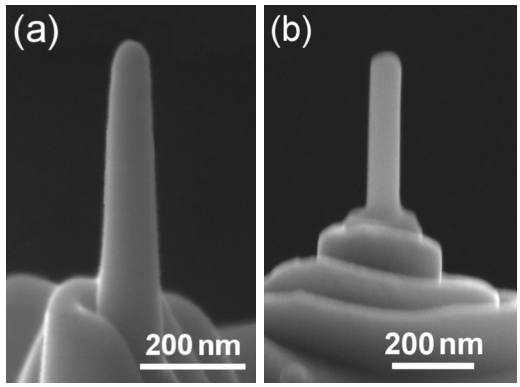

FIG. 1. SEM image of $Zr_{61.8}Cu_{18}Ni_{10.2}Al_{10}$ nanopillar made by FIB top milling (a) and further side polishing (b).

[a)]Author to whom correspondence should be addressed. Tel.: 31-50-363 4898. FAX: 31-50-363 4881. Electronic mail: j.t.m.de.hosson@rug.nl.

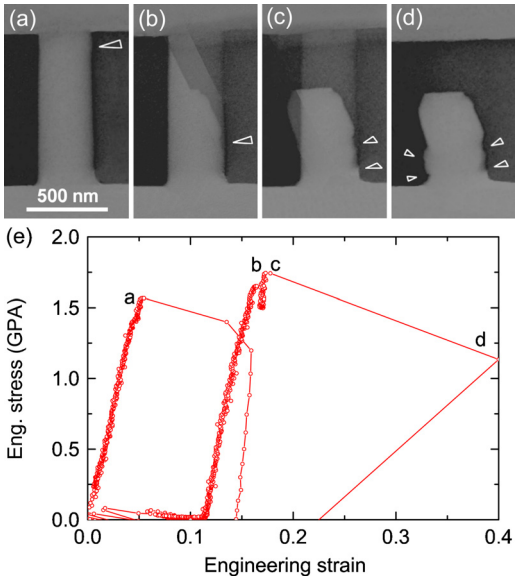

FIG. 2. (Color online) [(a)–(d)] Grabbed TEM video frames recording the deformation of a ∅460 nm $Zr_{61.8}Cu_{18}Ni_{10.2}Al_{10}$ MG taper-free pillar compressed under displacement-rate controlled mode, corresponding, respectively, to the deformation structure marked on the load–displacement curve (e). Open white arrows annotate SBs in pillars during and after compression.

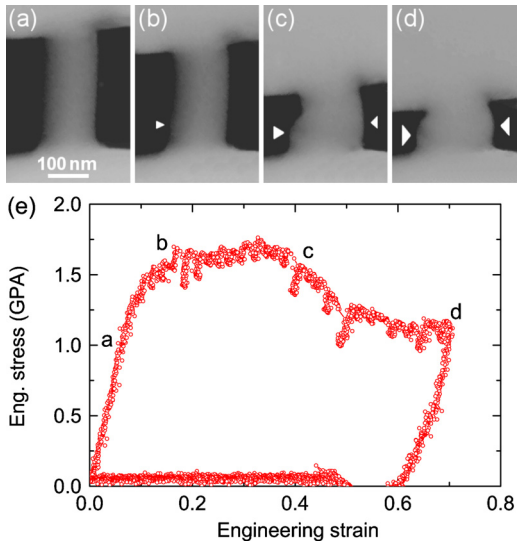

FIG. 3. (Color online) [(a)–(d)] Grabbed TEM video frames recording the deformation of a ∅140 nm $Zr_{61.8}Cu_{18}Ni_{10.2}Al_{10}$ MG taper-free pillar compressed under displacement-rate controlled mode, corresponding to different strain values marked in the load–displacement curve (e). Filled white arrows annotate bulging areas in pillars during compression. Sizes of arrows correspond to different bulging volumes.

with aspect ratio ranging between 3 and 4 were fabricated step by step by decreasing of FIB current on different milling stages. The final shape of the taper-free pillars has been achieved by FIB side polishing [Fig. 1(b)]. The uniform amorphousness of the FIB-milled nanopillars was verified by x-ray analysis and TEM observations.

In situ TEM compression experiments were performed using a Hysitron picoindenter TEM holder (Hysitron Inc., Minneapolis, MN, USA) equipped on JEOL 2010F TEM, with a diamond flat punch of 2 μm in diameter. The indenter has several unique features, which are particularly critical to the present study. First, it is integrated with a miniature capacitive load–displacement transducer permitting high resolution load and displacement measurements (resolution of ~0.3 μN in load, ~1 nm in displacement). In addition, a rapid instrument response and data acquisition rate (the controller is operating in a continuous loop and samples data at 20 kHz) allows discrete flow events to be well-resolved. The experiments were run in two typical control modes: displacement-rate control that shows a great sensitivity, and load control that has an advantage in evaluating sudden displacement jumps (SB offset). The displacement and/or load rate were programmed in such a way that a nominal strain rate of $\sim 10^{-2}$ s^{-1} is applied.

Figure 2 shows a sequence of frames grabbed from *in situ* recorded video of the compression of a $Zr_{61.8}Cu_{18}Ni_{10.2}Al_{10}$ pillar with a relatively large tip diameter of 460 nm and was compressed under displacement rate control. Due to the friction between the top part of the pillar and the indenter tip when deformation starts, small shear [Fig. 2(a)] the top part of pillar, subsequently two major and one top SBs are triggered simultaneously at a larger event [Figs. 2(b) and 2(c)]. They occur rapidly with a speed beyond the recording speed of the camera. With decreasing pillar diameters, the deformation behavior continues by showing shear banding. However, the amplitude of load drops (LDs), which represent a SB displacement, decreases significantly. In pillars with diameter of about 150 nm we observe no major or large shear displacements. It is considered that this diameter is the transition point between inhomogeneous and homogeneous behavior of pillar response to compression. Figure 3 shows the video frames recording the compressive deformation of a ∅140 nm pillar. Bulging was observed at about one third of its height close to the base and continued with increasing displacement. The deformation reached an engineering strain up to 70% without any visible shear banding or offset [Figs. 3(c) and 3(d)], but rather homogeneous flow at this scale. This phenomenon is in contradiction to the deformation behavior of pillars with large sizes (>∅300 nm), which showed an engineering strain not larger than 5% before a major shear displacement occurs.

It is assumed that with reducing pillar size the probability of interactions between the shear transformation zones (STZs) decreases and, therefore, the probability of major shear formation decreases as well. Accordingly there is a critical pillar size, which is the transition threshold between inhomogeneous and homogeneous behavior of amorphous pillars under compression. Figure 4(a) displays the elastically strained volume before shear banding versus the diameter of pillars. Assuming the same yielding strength of STZs, the stored energy in the elastically strained volume needed to initiate the first major shear banding is the same. It indicates that as soon as STZs concentration per volume unit is enough, major shear displacement occurs. However, we do not observe homogeneous deformation at large samples. Large pillars from 600 nm down to around 300 nm in diameter show an elastic deformation followed by a jerky-type deformation with transient shear banding events registered with large LDs in the load–displacement curve [see Fig. 2(e)], which are analogs to the intermittent bursts or slip avalanches observed in crystalline materials with a power-law size distribution.[19,20] With decreasing pillar diameter the apparent deformation mode shows a gradual transition from highly inhomogeneous to homogeneous behavior, as indicated by the hatched zone in Fig. 4(a). The yield stress of all

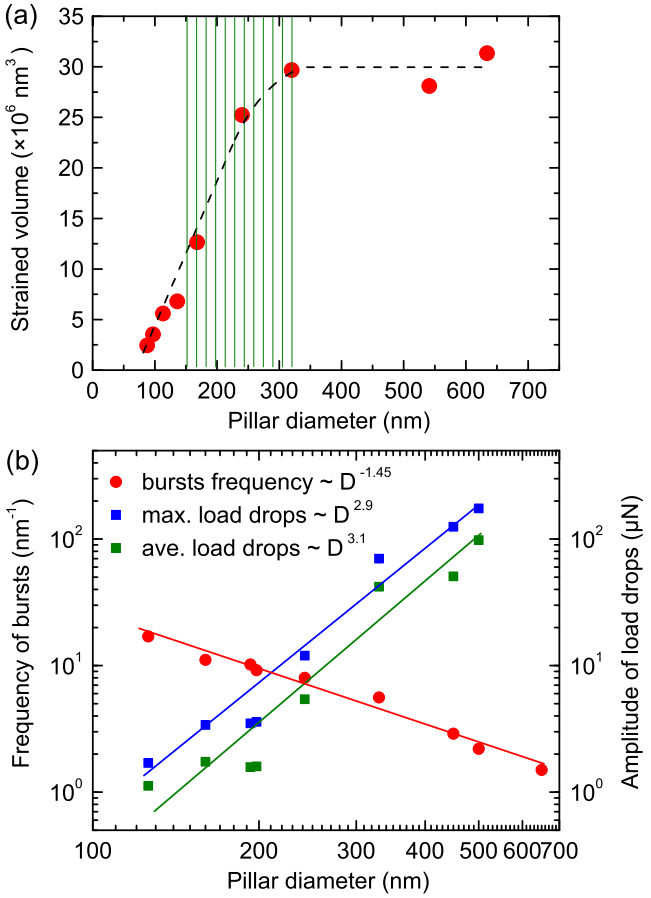

FIG. 4. (Color online) (a) Elastic strained volume vs pillar diameter of $Zr_{61.8}Cu_{18}Ni_{10.2}Al_{10}$ MG. (b) Mechanical characteristics and quantitative analysis as a function of pillar diameter: frequency of bursts and the amplitude of lord drops.

the pillars tested is size-independent, which is consistent with our previous work on tapered pillars.[17] For a review and details reference is made to.[21] The frequency of bursts increases rapidly with decreasing pillar diameter [power-law, Fig. 4(b)]. It indicates more frequently activated shear banding events, whereas the shear displacement carried by individual shear banding events decreases quickly, indicating suppression of SB propagation.

The observed LDs at constant displacement rate are triggered by the formation and propagation of multiple SBs. Amplitudes of LDs reveal that the shear displacement in thinner pillars proceeds more smoothly, while the stress decreases more steadily. At the smallest diameter of 110 nm, the amplitude of LDs is very small (~2 μN), whereas maximum load is still considerably high (~10 μN). The ratio between average LD and maximum load for ~100 nm pillars equals 8–10. This ratio decreases down to 1 for larger pillar diameters, which shows the propagation of a major SB to the edge of the pillar. This is caused by changes in the mechanism of plastic behavior with decreasing pillar diameter. During compression of micron pillars ductility appears due to distinctive structure of the BMGs. The shear transformation zones occur preferentially in soft regions in BMGs and evolve into SBs upon loading. Consequently, numerous SB nuclei are formed concurrently in the soft regions. Because the soft regions cannot carry much plastic strain due to SB multiplication processes, any further deformation has to proceed in hard regions so that higher plasticity is still attainable on a large scale. With pillar size on the scale of hundred of nanometers, this mechanism is no longer applicable, due to the decrease in the quantity and interaction of soft regions.

In summary, *in situ* compression tests of taper-free micro-/nanopillars of $Zr_{61.8}Cu_{18}Ni_{10.2}Al_{10}$ MG with tip diameters ranging from 600 to 90 nm show predominant inhomogeneous and intermittent plastic flow characterized by shear banding events. The deformation is defect-nucleation-controlled in larger pillars but becomes propagation-controlled in smaller pillars. Pillars with a diameter smaller than 150 nm show a homogeneous flow behavior without shear banding during compression. It is concluded that larger overlap of stress fields of flow defects in smaller pillars (samples) plays a crucial role for the ductile behavior. Quantitative analysis of load–displacement curves have revealed a strong size effect of nanopillars under compression and confirmed the existing of transition threshold from inhomogeneous to homogeneous deformation behavior.

We acknowledge the Netherlands Organization for Research (Physics division, FOM-Utrecht, The Netherlands) and the Materials innovation institute M2i for financial support to the joint fundamental research project No. M62.7.08SDMP13.

[1]W. Klement, R. H. Wilens, and P. Duwez, Nature (London) **187**, 869 (1960).
[2]C. A. Schuh, T. C. Hufnagel, and U. Ramamurty, Acta Mater. **55**, 4067 (2007).
[3]M. Chen, Annu. Rev. Mater. Res. **38**, 445 (2008).
[4]J. Th. M. De Hosson, Microsc. Res. Tech. **72**, 250 (2009).
[5]J. T. M. De Hosson, C. Q. Chen, Y. T. Pei, V. Ocelik, and D. Matthews, TMS Annual Meeting and Exhibition, 2010, Feb. 14-18, 2010, Seattle.
[6]C. G. Tang, Y. Li, and K. Y. Zeng, Mater. Lett. **59**, 3325 (2005).
[7]Z. W. Shan, J. Li, Y. Cheng, A. Minor, S. A. Syed Asif, O. L. Warren, and E. Ma, Phys. Rev. B **77**, 155419 (2008).
[8]Q. Zheng, S. Cheng, J. Strader, E. Ma, and J. Xu, Scr. Mater. **56**, 161 (2007).
[9]C. Lee, J. Huang, and T. Nieh, Appl. Phys. Lett. **91**, 161913 (2007).
[10]S. Cheng, X. Wang, H. Choo, and P. Liaw, Appl. Phys. Lett. **91**, 201917 (2007).
[11]B. Schuster, Q. Wei, M. Ervin, S. Hruszkewycz, M. Miller, T. Hufnagel, and K. T. Ramesh, Scr. Mater. **57**, 517 (2007).
[12]Y. Lai, C. Lee, Y. Cheng, H. Chou, H. Chen, X. Du, C. I. Chang, J. C. Huang, S. R. Jain, J. S. C. Jang, and T. G. Nieh, Scr. Mater. **58**, 890 (2008).
[13]C. Volkert, A. Donohue, and F. Spaepen, J. Appl. Phys. **103**, 083539 (2008).
[14]B. Schuster, Q. Wei, T. Hufnagel, and K. Ramesh, Acta Mater. **56**, 5091 (2008).
[15]A. Dubach, R. Raghavan, J. LoËffler, J. Michler, and U. Ramamurty, Scr. Mater. **60**, 567 (2009).
[16]C. Q. Chen, Y. T. Pei, and J. Th. M. De Hosson, Acta Mater. **58**, 189 (2010).
[17]C. Q. Chen, Y. T. Pei, and J. T. M. De Hosson, Philos. Mag. Lett. **89**, 633 (2009).
[18]J. J. Lewandowski, W. H. Wang, and A. L. Greer, Philos. Mag. Lett. **85**, 77 (2005).
[19]J. E. Carsley, A. Fisher, W. W. Milligan, and E. C. Aifantis, Metall. Mater. Trans. A **29**, 2261 (1998).
[20]M. Zaiser and E. C. Aifantis, Int. J. Plast. **22**, 1432 (2006); J. Mech. Behav. Mater. **14**, 255 (2003).
[21]J. R. Greer and J. T. M. De Hosson, Prog. Mater. Sci. **56**, 654 (2011).